EFFECT OF ORGANIC BOUND Na GROUPS ON PYROLYSIS AND CO$_2$-GASIFICATION OF ALKALI LIGNIN

Da-Liang Guo,[a] Shu-Bin Wu,[a,*] Rui Lou,[a] Xiu-li Yin,[b] and Qing Yang[b]

To investigate the effect of organic bound Na groups on pyrolysis and gasification behaviors of alkali lignin, an experimental study was carried out by Thermogravimetric Analyzer coupled with Fourier Transform Infrared Spectrometry (TG-FTIR). Acid precipitated lignin (APL) and Alkali soluble lignin (ASL) were selected as the testing samples, and physiochemical properties were studied by FTIR, ^{1}H NMR, and SEM analyses. The research results showed that the pyrolysis and gasification characteristics of alkali lignin depended on phenolic sodium (-CONa) and carboxylate sodium (-COONa) groups (PCSG). In pyrolysis stage, PCSG improved the yields of alcohols and hydrocarbons but inhibited benzenes. During gasification stage, in the present of PCSG, the peak value of gasification rate increased, yet the initial gasification temperature decreased. Meanwhile, CO releasing was relatively concentrated and intensively increased from 37 min (740 ^{o}C) to 42 min (840 ^{o}C).

INTRODUCTION

Pyrolysis and gasification of biomass-containing wastes from industrial resources have great potential to reduce fossil fuel demand for fuels and chemical feedstocks (Naqvi et al. 2010). In the pulp and paper industry, large quantities of lignocellulosic biomass have been used, and the by-products resulting from the industry including bark, black liquor, and alkali lignin are one of the major biomass resources that can be further used for energy (Joelsson and Gustavsson 2008). However, the high content of sodium salt has a significant effect on the pyrolysis and gasification characteristics of lignin (Kumar 2009).

In the soda pulping process, sodium hydroxide is used as the cooking chemical to dissolve lignin. Chemical action and solubilization make Na$^+$ connect with phenolic hydroxyl groups (-OH) and carboxylic acid groups (-COOH) of lignin by chemical bonds, forming PCSG (Connolly 2006). Thus, the form of PCSG can be considered as a part of alkali lignin organic substance. Meanwhile, the chemical and physical forms of sodium are crucial factors influencing the pyrolysis and gasification behaviors (Quyn et al. 2002). An early work by Cerfontain (1988) concluded that PCSG was an important vehicle for organic carbon gasification. Sams and Shadam (1986) proposed a mechanism for the gasification of organic carbon catalyzed with an alkali carbonate by CO$_2$. They

found that the formation of the catalytic functional groups from the alkali carbonate and the organic carbon proceed around $250\,^{\circ}C$. From this aspect, PCSG plays an important role in pyrolysis and gasification of alkali lignin. Up to now, pyrolysis and gasification of black liquor with catalytic alkali carbonate have been extensively studied (Li 1998; Whitty et al. 1998; Sricharoenchaikul et al. 2003). In addition there has been some research about alkali lignin (Ferdous et al. 2002; Yang et al. 2007); the cited authors concluded that pyrolysis and gasification of alkali lignin are complex processes. Different factors such as the reaction temperature, heating rate, and carrier gas flow rate had been studied extensively, but there is very limited literature available on the effect of alkali metal combined with organic structure on the lignin pyrolysis and gasification.

Thermogravimetric analysis (TGA) is often used to study the thermal behavior and kinetics parameters under inert gases. However, the composition of products in each weight loss step cannot be obtained by TGA alone. On the other hand, Fourier Transform Infrared Spectroscopy (FTIR) results can be used to evaluate the functional groups and prove the existence of some volatiles (Bassilakis et al. 2001). The aim of this paper is to investigate the effect of PCSG on alkali lignin pyrolysis and CO_2 gasification by using the technique of online TG-FTIR. TGA is adopted to keep a detailed recording of the mass loss data, and FTIR is used to predict the product evolution pattern and yield.

EXPERIMENTAL

Materials

Black liquor used in this study was obtained from a wheat straw soda-AQ pulp mill in Shandong Province. Black liquor sample was filtered through a 200-mesh screen to remove any suspended matter.

Acid precipitated lignin (APL), without PCSG, was separated from the black liquor sample by acidification with 1N H_2SO_4 to pH 2.0. Precipitated solids were filtered from the solution, washed thoroughly with distilled water, and dried. Subsequently, the dried solids were dissolved in 1,4-dioxane, then reclaimed by rotary evaporation of solvent under vacuum and dried to remove inorganic impurities. Finally, the absolute dry APL was used for this research.

Alkali soluble lignin (ASL), with PCSG, was prepared by using NaOH solution to dissolve APL. A known amount of APL solid was first added into a beaker. Then 0.1 mol/L NaOH solution was loaded into the beaker, until the APL sample was completely dissolved. The process of addition needed to be as gradual and slow as possible in order to avoid loading excessive NaOH. Finally, the lignin solution was dried, and then the ASL sample was obtained.

Table 1. Utimate and Proximate Analysis of the Materials

Materials	Proximate analysis (%)		Ultimate analysis (%)				Na (ppm)	Q_{HHV} (MJ/kg)
	Ashes	Volatiles	C	H	O[*]	N		
APL	5.95	87.83	56.01	8.54	35.34	0.11	-	22.87
ASL	21.93	72.48	48.31	3.32	48.23	0.14	19405	13.77

*Oxygen content was determined by difference.

The CHNS elemental analysis of the samples was performed with an elemental analyzer (Vario-I Germany). Component analysis on the feedstock was done according to the national standard methods and the literature (Shi et al. 2003). The determination of mineral composition of the feedstock with digestion method and determined by ICP-AES. Results of ultimate and proximate analysis of the samples are shown in Table 1. From Table 1, the marked difference of constituents between APL and ASL were the content of ash and Na.

Methods

Infrared spectra of APL and ASL were recorded on an infrared spectrometer (FTIR Nexus series, Thermo Nicolet Company US). The samples were pressed with chromatography grade KBr, and the transparent films made by using a type Tianjin Fw-4 press machine were determined.

The ^{1}H NMR spectra were obtained using a Bruker DRX-400 spectrometer operating in the FT mode at 74.5 MHz. At room temperature, the lignin sample (20 mg for ^{1}H, 200 mg for ^{13}C) was dissolved in 1 mL DMSO-d6 (99.8% D).

The surface morphology of APL and ASL were studied by using an S-3700N (Japan, Hitachi) SEM. The signal was transformed by a second electron microscopic image at a working distance 19.8 mm and accelerating voltage 10kV. The magnifications were 2000 and 10000.

A Jupiter thermogravimetric analyzer STA 449 F3 was used in this work. A Thermo Electron Corporation Fourier Transformation Infrared Spectrometer TENSOR 27 was used to collect evolved gases from TGA. Resolution in FTIR was set at 4 cm^{-1}, spectrum scan frequency at 20 times per minute, and the spectral region in the range 4000 to 667cm^{-1}. The TGA and FTIR were connected by a pipe, and the Fourier Transform Infrared Spectrometer gas cell was already preheated to 150 ^{o}C before each experiment.

The experiments were done on TGA at a heating rate of 20 °C/min within the temperature range from 50 to 1000 ^{o}C. High purity N_2 was used as carrier gas with a flow rate of 20 mL/min during pyrolysis; CO_2 was used as gasifying agent with a flow rate of 40 ml/min during gasification. The weight of sample was required to be less than 10 mg.

RESULTS AND DISCUSSION

Structure Characterization of APL and ASL

FT-IR and ^{1}H NMR spectra of APL and ASL are shown in Figs. 1 and 2, respectively. From Fig.1, the characteristic bands locating at 1427, 1461, 1512, and 1604 cm^{-1} indicated the existence of aromatic rings and C–H bonds (Sun and Tomkinson 2001). The band at 3417 cm^{-1} originated from the O-H stretching vibration in aromatic and aliphatic OH groups. The bands at 2932 and 2847 cm^{-1} arose from the C-H stretching and asymmetric vibrations of CH_3 and CH_2, respectively (Yuan et al. 2009). Moreover, the bands in the region of 1000 and 1400 cm^{-1} represented the existence of C–O or C–H, while the bands in the region of 1226 cm^{-1} indicated the appearance of aromatic phenyl C–O. Therefore, the aromatic structure of APL was not changed during the process of ASL formation.
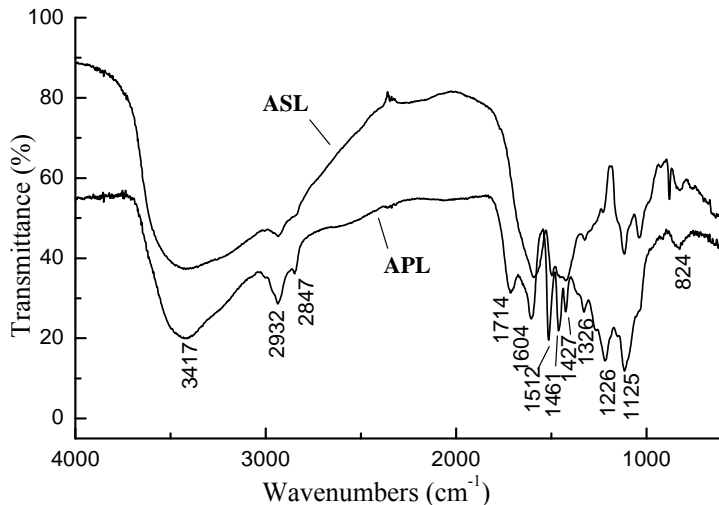
Fig. 1. FTIR spectra of APL and ASL

However, there was a difference between APL and ASL in the absorption at 1714 cm^{-1} which corresponded to the unconjugated carbonyl stretching. The spectrum of APL exhibited a strong absorption at 1714 cm^{-1}, while this was not found for ASL.

^{1}H NMR spectroscopy revealed more details about the structural characteristics of APL and ASL, as shown in Fig. 2a) and b). The region from 6.2 to 8.0 ppm corresponded to the protons in the aromatic region (Ghatak et al. 2010). The region 3.2 to 3.9 ppm was attributed to the protons in methoxyl. Signal integrations between 0.0 and 1.6 ppm originated from the β-H (hydrogen attached to the β-C) and hydrogen in non-oxygenated aliphatic region (Ghatak 2008). From Fig. 2a), APL had a larger proportion of β-H than ASL, which indicated higher occurrence of β-O-4 type entities. Compared with ASL, APL had larger proportion of aromatic protons by signal integrations between 6.2 and 8.0 ppm (Fig. 2a)). This was indicative of lower extent of substituent groups and linkages through the aromatic ring for APL. The signals at 2.5 ppm arose from DMSO.
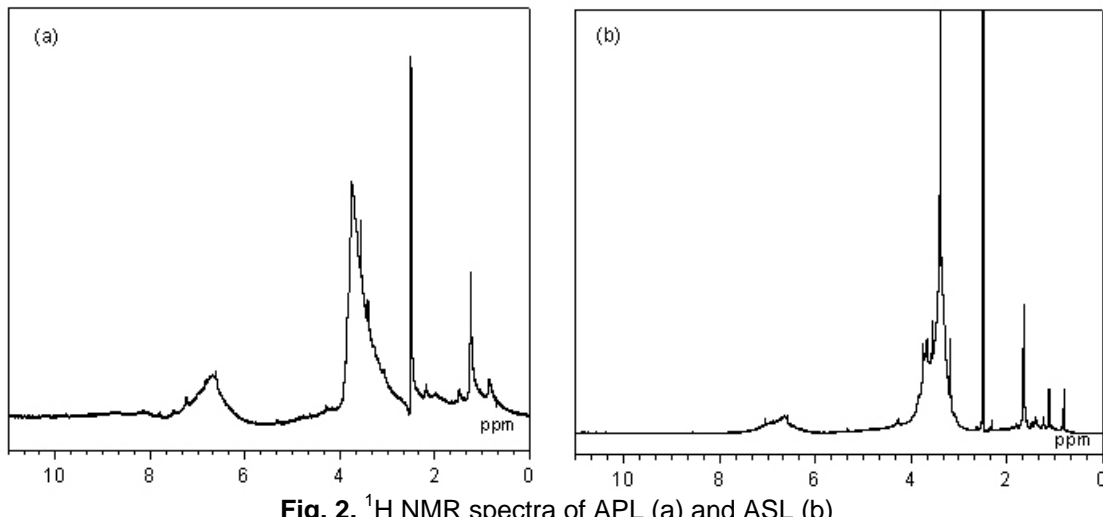
Fig. 2. ^{1}H NMR spectra of APL (a) and ASL (b)

SEM Analysis of APL and ASL

Morphology of APL with and without alkali treatment was investigated by scanning electron microscope (SEM), as shown in Figs. 3a), b) and c), d).

(a) **APL×2K**

(b) **APL×10K**

(c) **ASL×2K**

(d) **ASL×10K**
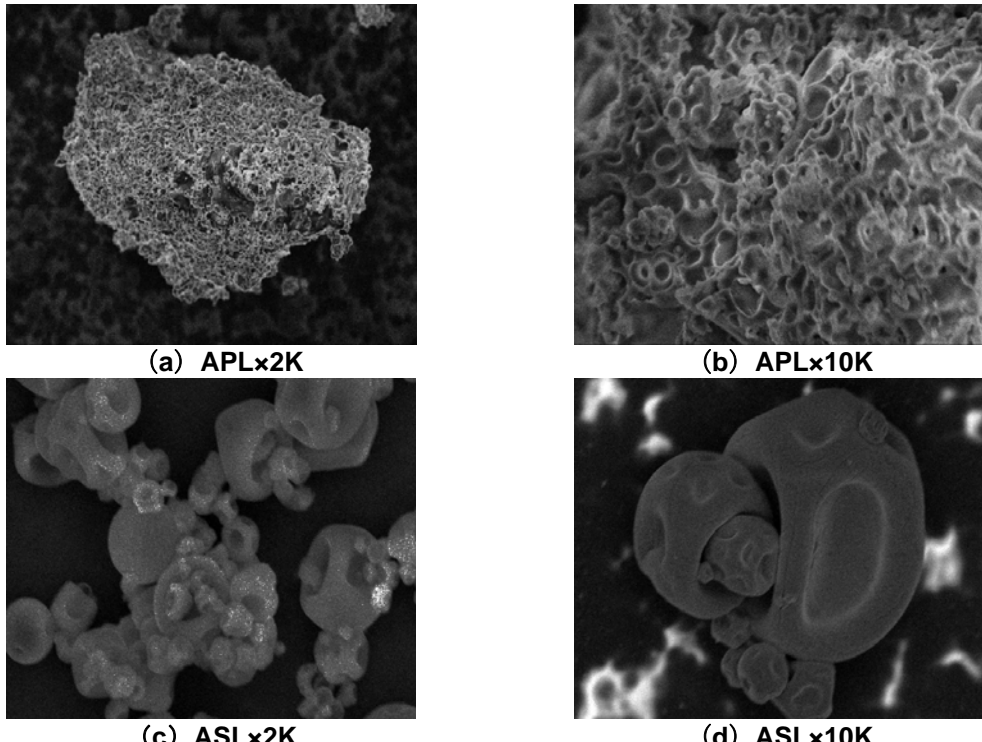
Fig. 3. SEM micrographs of APL and ASL

From Fig. 3a) and c), it can be observed that APL had an irregular structure, whereas ASL was ball-shaped or elliptical. Figure 3b) and d) show the surface topography of APL and ASL. The surface morphology of APL was porous and arabesquitic (Fig. 3b)). After alkali loading, ASL showed a regular shape with a smooth surface. It can be concluded that the morphology of APL and ASL were different. Sharma et al. (2004) reported that surface topography of a sample had an effect on the pyrolysis characterization of lignin. Therefore, the different morphology was one of reasons that APL and ASL had different characteristics of pyrolysis and CO_2 gasification.

TG and DTG Analysis

TG curves of APL and ASL are shown in Fig. 4a), and the rates of thermal degradation (DTG curves) are presented in Fig. 4b).

From Fig. 4a), it was shown distinctly that the pyrolysis and gasification of APL could be approximately described by two stages. The first stage between 200 and 600 ^{o}C (10 and 30 min) was responsible for the pyrolysis of APL, accounting for 52.18% weight loss with a maximum mass loss rate at 400 ^{o}C (Fig. 4b)). The second stage from 900 to 1000 ^{o}C (45 to 60min) was the main gasification stage, accounting for a weight loss of 29.40% with a maximum rate of thermal degradation at 1000 ^{o}C (Fig. 4b)).

For ASL, TG results presented three distinct phases of weight loss. The first weight loss process was due to the moisture of ASL accounting for 5.19% weight loss with the maximum mass loss rate at 160 ^{o}C. Subsequently the second and third process could be ascribed to the main pyrolysis and gasification of ASL accounting for 24.45% and 22.50% with a maximum rate of thermal degradation at 350 and 800 ^{o}C, respectively.

The DTG results revealed that the reaction rate during APL pyrolysis was faster than that of gasification. However, the reaction rate of ASL during pyrolysis was slower than that of gasification. This phenomenon may be attributed to the PCSG in ASL, which was reasonably in agreement with the results reported by Lv et al. (2010) concerning the effect of alkali and alkaline earth metallic (AAEM) species on biomass pyrolysis and gasification. Therefore, the gasification activity of ASL was a result of the interaction between alkaline metal and lignin.
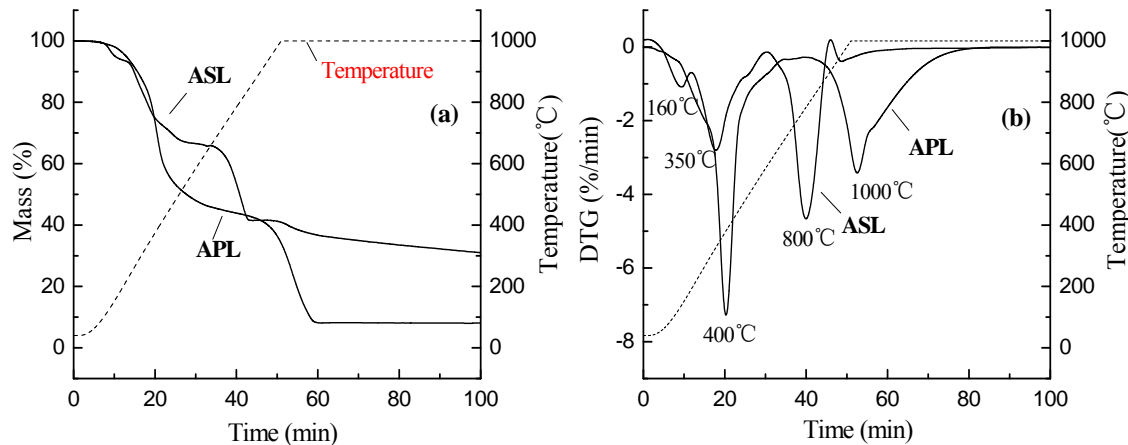
Fig. 4. TG and DTG Curves of APL and ASL

Effect of PCSG on the Volatile Products

Three dimensional plots of the FTIR spectra obtained from gas evolution during the pyrolysis and CO_2 gasification of APL and ASL are shown in Fig.5. From Fig. 5 it can be observed that the main gas products evolving from APL and ASL pyrolysis were CO, CH_4, H_2O, benzenes, hydrocarbons, alcohols and phenols, aldehydes, and ketones (C=O) (Liu et al. 2008; Bassilakis et al. 2001; Zhu et al. 2008; Lv et al. 2010). The release of these products mainly occurred at low temperatures, corresponding to the main pyrolysis temperature zone in the TG curve (Fig. 4a)).

Based on the maximum mass loss rate of DTG curves, three levels of temperature were selected to investigate the effect of PCSG on the volatile products. The spectra of volatiles released at 180, 400, and 1000 ^{o}C for APL are shown in Fig. 6a), b), and c), respectively. For ASL, Fig. 7a), b), and c) corresponded to that of 160, 350, and 800 ^{o}C, respectively. The characteristic bands of H_2O at 3500-3964 and 1300-1800 cm^{-1} were attributed to the release of bound water during the initial pyrolysis stage, as shown in Figs. 6a) and 7a). In main pyrolysis stage, evolution of H_2O was caused by the cracking of aliphatic hydroxyl groups in the side chains (Liu et al. 2008) (Fig. 6b) and 7b)). When the reaction progressed into the gasification stage, the absorption band of H_2O for APL was still present (Fig. 6c)).

(a) ASL   **b) APL**
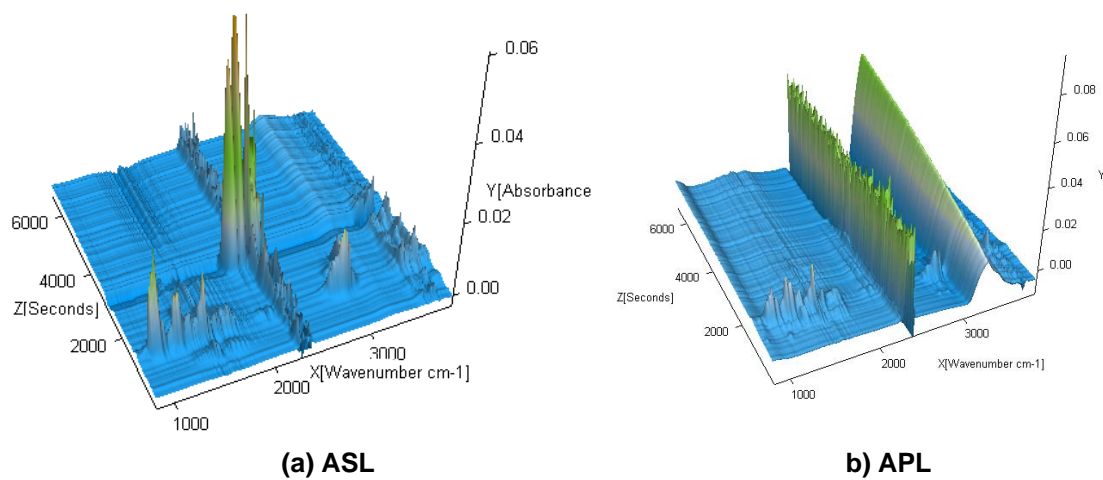
Fig. 5. 3D FTIR spectra from pyrolysis and CO_2 gasification of ASL and APL
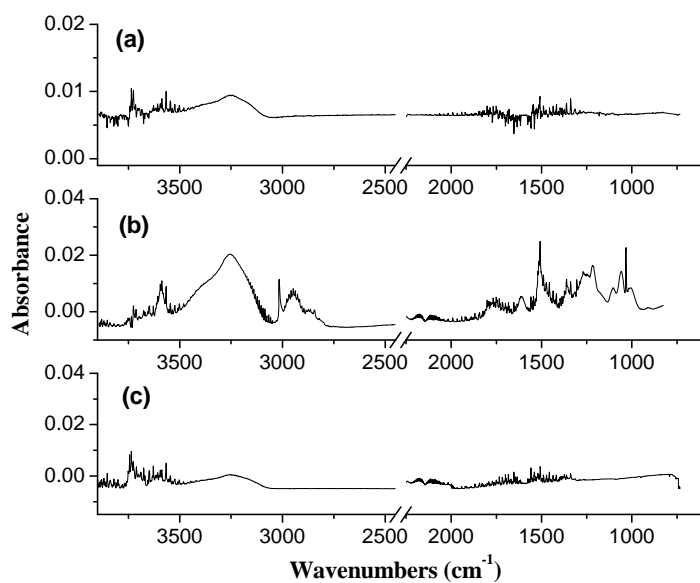
Fig. 6. FTIR spectra of APL pyrolysis and gasification

When reactions proceeded into the main pyrolysis stage, more gaseous products were released (Fig. 6b) and 7b)). The maximum mass loss rate was mostly attributable to the release of volatiles (Yuan et al. 2009), such as H_2O, alcohols, phenols, benzenes, and hydrocarbons etc. The characteristic bands of alcohols between 1040 and 1180 cm^{-1} indicated that it was released mostly over this temperature range. An intense signal cluster, centered around 1517 cm^{-1} (C=C stretching vibrations) and accompanied by signals at 1772 cm^{-1} (C=O stretching vibrations), strongly indicated the presence of some organic compounds, consisting of aldehydes, esters, and acids (Lv et al. 2010). The most significant band was O–H at 1300-1400 cm^{-1}, corresponding to the main presence of phenols (Liu et al. 2008). From Fig. 6b) and 7b), the absorption intensity of phenols for

APL was stronger than that for ASL. The bands at 2850-3200 cm^{-1} represented the existence of hydrocarbons (Sun and Tomkinson 2001). ASL showed stronger absorption intensity of hydrocarbons than APL. The main reason might be that sodium hydroxide lead to a remarkable reduction of the C-H bond energies of lignin (Su et al. 2010).

The absorbance peak of CO (2185 cm^{-1}) appeared in the main pyrolysis stage, although in quite small amounts (Fig. 6b) and 7b)). However, a considerable amount of CO is released from ASL in gasification stage (Fig. 6c) and 7c)). This might be attributed to the catalysis of PCSG on gasification reaction (Kumar 2009). Therefore, the yield of CO may be applied to estimate the effect of PCSG on lignin gasification reaction.
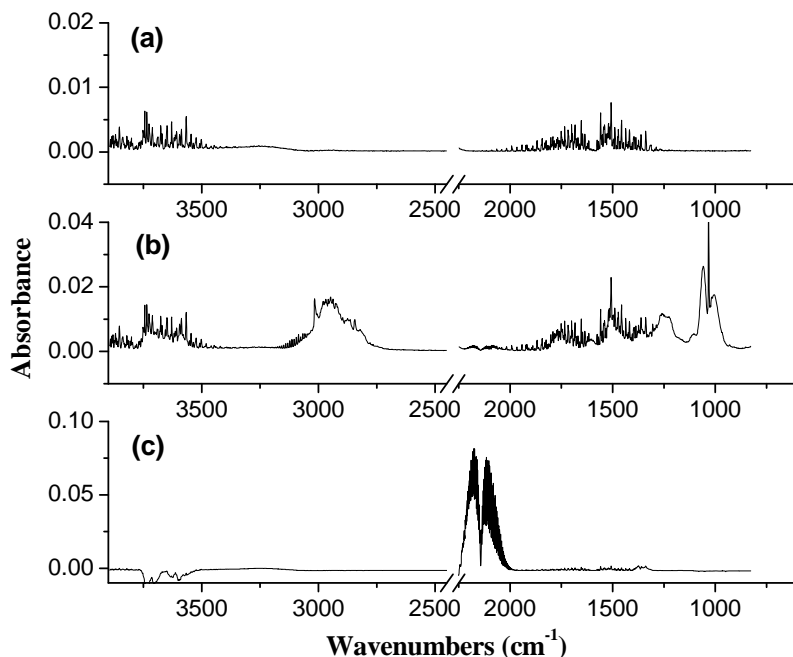
Fig. 7. FTIR spectra of ASL pyrolysis and gasification

Effect of PCSG on Mechanism of Products Forming

The FTIR spectrometer cannot present the concentration of products other than the absorption intensity as a function of time. According to the widely applied Lambert-Beer law, the absorption intensity at specific wavenumbers is linearly dependent on gas concentration (Bassilakis et al. 2001). So the variation of absorption intensity in the whole process can reflect the tendency of product yields of the gas species. By integration of the absorption intensity in Fig. 8 (a)-h)), the relative yields of the main products were quantified and compared.

As shown in Fig. 8 a) and b), the evolution profile of CH_4 for APL had four strong peaks; ASL only had two weak peaks. The evolution peaks of CH_4 at low temperature (400 ^{o}C) were caused mainly by the cracking of the methoxyl group (–OCH_3) on the aromatic rings, while at high temperature might be attributed to the decomposition of the methylene groups (–CH_2–) and to the hydrocarbon skeleton, after deoxygenation (Lv et al. 2010). It can be found that a large number of secondary reactions to generate CH_4

occurred during APL pyrolysis, while this was not obvious for ASL. The reasons behind the variable results are not clear, but are currently under investigation. The authors conjectured that PCSG decreased the required reaction temperature of gasification, and thus limited the reaction of pyrolysis.

Figure 8 c) and d) indicate that the generation of aldehydes and ketones was more concentrated than the other volatiles. The release of aldehydes and ketones started at 15 min (300 $^{\circ}$C), finished at 30 min (600 $^{\circ}$C), and reached a maximum at 21 min (420 $^{\circ}$C) and 25 min (500 $^{\circ}$C) for APL and ASL, respectively. From Fig. 8 c) and d), it can be found that the release profiles of aldehydes and ketones for APL showed a pattern similar to that of ASL, except that their release rates were much higher. The absorption intensity of aldehydes and ketones for ASL were lower than APL. This indicated that the yields of aldehydes and ketones released from APL were higher than ASL. It was worth noting that the release peak temperature (420 °C) was a little higher than that of the first weight loss peak (400 °C) (Fig. 4b)), due to the transitional delay between TGA and FTIR. Similar appearances can be seen in Fig. 8 e)-h).

The formation of benzenes, shown in Fig. 8 e) and f), probably arose from the breaking of lateral C–C bonds in the lignin structure. During APL pyrolysis, the formation profile of benzenes had four peaks between 10 min (200 °C) and 25 min (500 $^{\circ}$C). For ASL, the formation profile of benzenes had only one strong peak, started at 20 min (400 °C), reaching a maximum at 22 min (440°C), and then decreasing dramatically until 25 min (500°C) followed by a slow continuous decrease. Meanwhile, the absorption intensity of benzenes from ASL was also lower than APL. By integration of the evolution profiles of aldehydes & ketones, and benzenes, the evolution patterns of aldehydes and ketones were similar with that of benzenes for ASL pyrolysis, whereas different for APL (Fig. 8 c)-f)).

Figure 8 g) and h) revealed that a small quantity of CO was generated from APL and ASL pyrolysis. During APL pyrolysis, the generation of CO began at 200 $^{\circ}$C and finished at about 1000 $^{\circ}$C. However, in the present of PCSG, CO releasing from the process of ASL pyrolysis and CO_2 gasification was relatively concentrated and intensively increased from 37 min (740 $^{\circ}$C) to 42 min (840 $^{\circ}$C). This data strongly supported the mechanisms proposed by Sams and Shadman (1986) for the gasification of organic carbon catalytic with an alkali carbonate by CO_2 (Eqs. 1-4).

$$\text{-COONa} + \text{C(s)} \rightarrow \text{-CONa} + \text{CO(g)} \tag{1}$$

$$\text{-CONa} + \text{C(s)} \rightarrow \text{-CNa} + \text{CO(g)} \tag{2}$$

$$\text{-CNa} + \text{CO}_2\text{(g)} \rightarrow \text{-CONa} + \text{CO(g)} \tag{3}$$

$$\text{-CONa} + \text{CO}_2\text{(g)} \rightarrow \text{-COONa} + \text{CO(g)} \tag{4}$$

For the mechanism of catalytic gasification with PCSG, the reactions (1) and (2) can be conceived as the reduction of the PCSG catalytic sites by the organic carbon. The reactions (3) and (4) can be identified as the oxidation of the Na-C catalytic sites by CO_2.

The catalytic gasification reactions are best described by the combination of Eq (1) and (4) as follows:

$$-COONa + C(s) \rightarrow -CONa + CO(g) \qquad (1)$$

$$-CONa + CO_2(g) \rightarrow -COONa + CO(g) \qquad (4)$$

$$\overline{C (s) + CO_2 (g) \rightarrow 2CO (g)} \qquad (5)$$
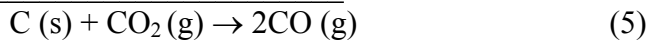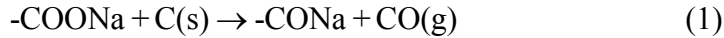
According to Connolly (2006) the reaction rate of PCSG with CO_2 was far faster than that of PCSG with organic carbon, so Eq. (1) will be the rate determining step of the gasification of ASL. For APL, without the present of PCSG, the gasification reaction should only be represented as Eq. (5), which is highly endothermic and will not proceed until significantly high temperatures are reached (Sams and Shadman 1986).
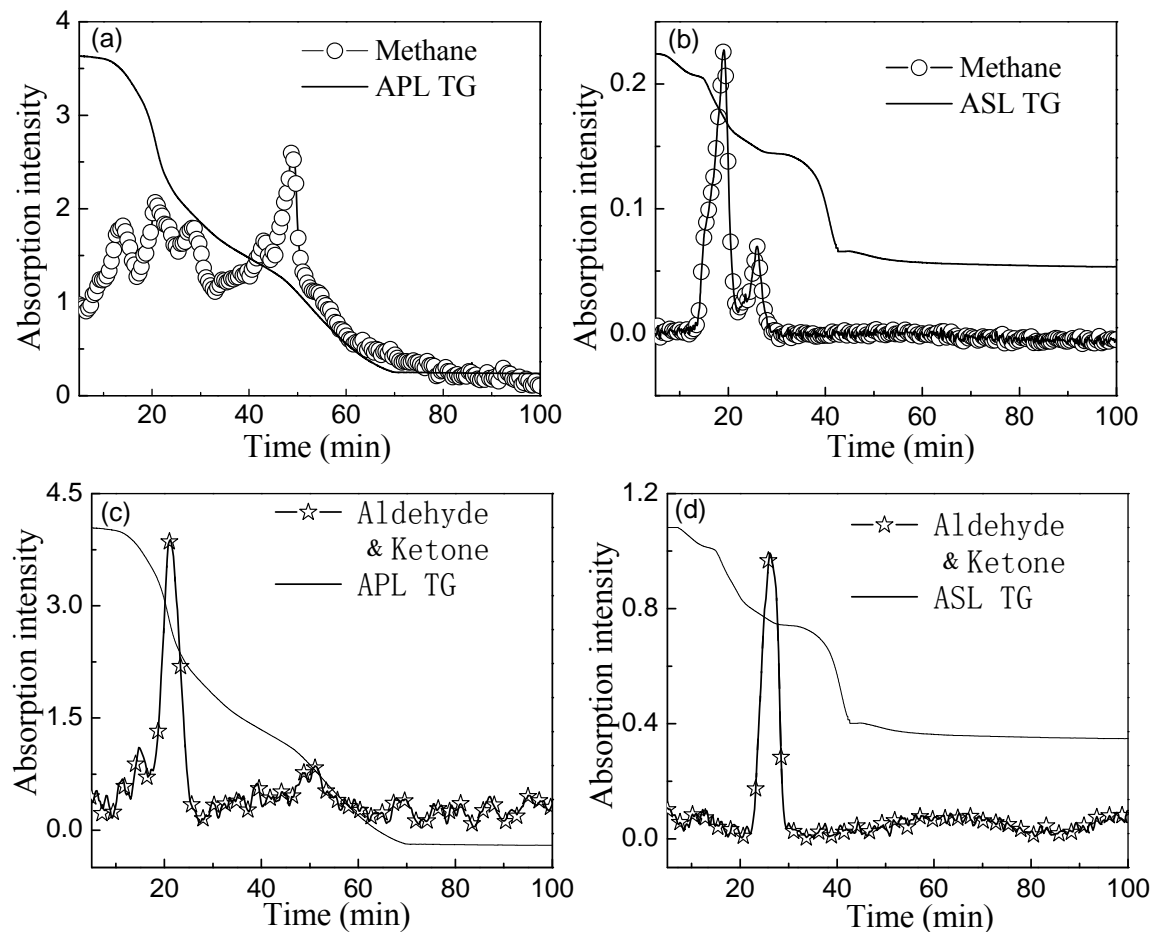
Fig. 8A. FTIR profiles of gas product evolving from APL and ASL pyrolysis and gasification
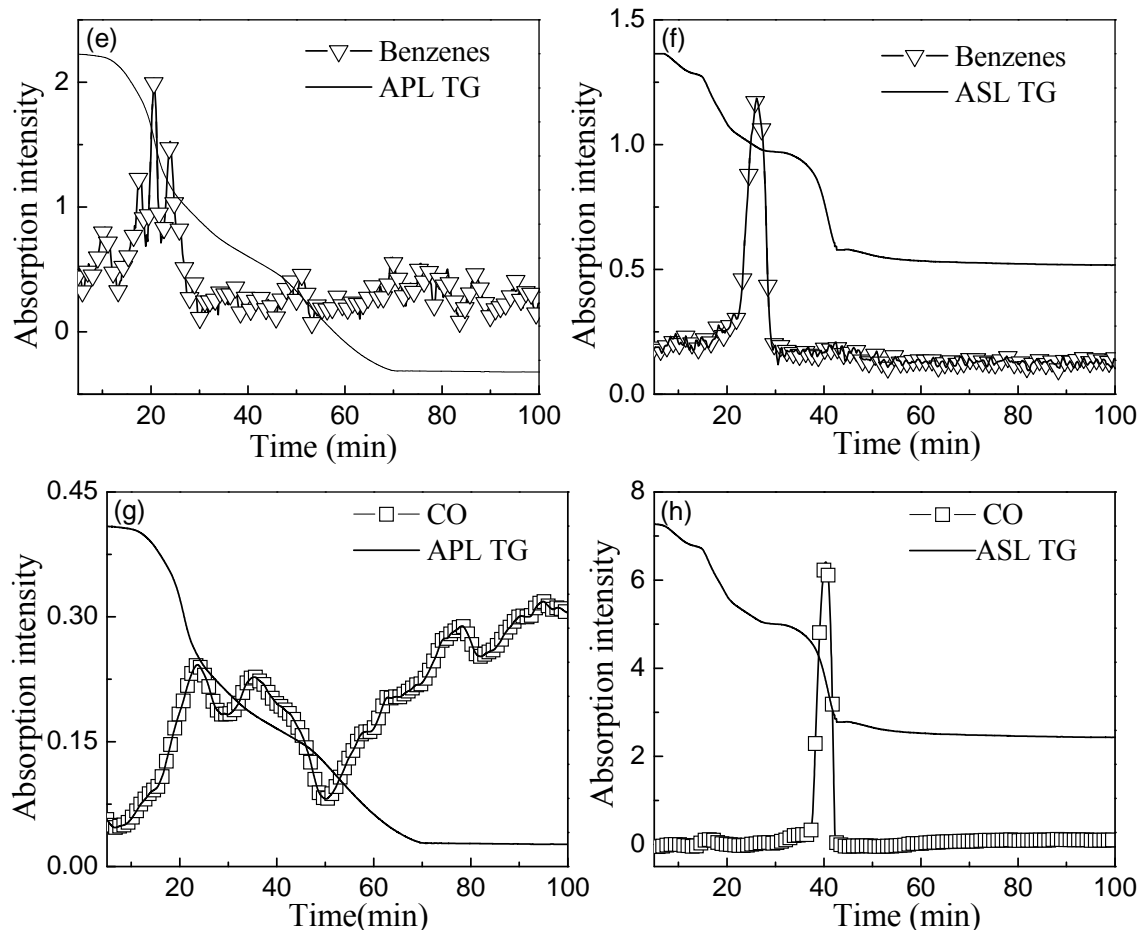
Fig. 8B. FTIR profiles of gas product evolving from APL and ASL pyrolysis and gasification

CONCLUSIONS

PCSG have a significant effect on pyrolysis and gasification reactions. The following conclusions can be drawn from the experimental results:

- FTIR and ^{1}H NMR spectra of APL and ASL showed that H in -OH and -COOH groups were replaced with Na. Therefore, the aromatic structure of alkali lignin was not destroyed in the process of APL and ASL preparation. SEM results indicated that the morphological characteristics of APL and ASL were different. APL had an amorphous structure, whereas ASL were mostly ball-shaped and elliptical.

- TGA curves revealed that the thermogravimetric behaviors of APL and ASL were different. In the presence of PCSG, the temperature of the maximum gasification rate decreased from 1000 to 800 °C; meanwhile, the peak value of the maximum gasification rate obviously increased.

- For APL pyrolysis, there were strong absorption intensities of CH_4, aldehydes, and ketones, while these were not obvious for ASL. For ASL pyrolysis, there were strong

absorption intensities of alcohols and phenols, but APL was not obvious. It can be concluded that the effect of PCSG on the pyrolysis products mainly varied in amounts but not in species.

● The reduction of PCSG sites by organic carbon and the subsequent oxidation of these sites by CO_2 can be used to explain the catalytic gasification mechanism for ASL gasification. In the presence of PCSG, the release of CO was relatively concentrated and intensively increased from 37 min (740 $^{\circ}$C) to 42 min (840 $^{\circ}$C).

ACKNOWLEDGMENTS

REFERENCES CITED

Bassilakis, R., and Carangelo, R. M. (2001). "TG-FTIR analysis of biomass pyrolysis," *Fuel* 80(12), 1765-1786.

Connolly, T. S. (2006). "CO$_2$ pyrolysis and gasification of kraft black liquor char," The University of Maine.

Cerfontain, M. B., Kapteijn, F., and Moulijna, J. A. (1988). "Characterization of alkali carbonate catalysts for carbon gasification with ^{18}O labeled CO$_2$," *Carbon* 26(1), 41-48.

Ferdous, D., Dalai, A. K., Bej, S. K., and Thring, R. W. (2002). "Pyrolysis of lignins: Experimental and kinetics studies," *Energy & Fuels* 16(6), 1405-1412.

Ghatak, H. R., Kundu, P. P., and Kumarc, S. (2010). "Thermochemical comparison of lignin separated by electrolysis and acid precipitation from soda black liquor of agricultural residues," *Thermochimica Acta* 502(1-2), 85-89.

Ghatak, H. R. (2008). "Spectroscopic comparison of lignin separated by electrolysis and acid precipitation of wheat straw soda black liquor," *Industrial Crops and Products* 28(2), 206-212.

Joelsson, J., and Gustavsson, L. (2008). "CO$_2$ emission and oil use reduction through black liquor gasification and energy efficiency in pulp and paper industry," *Resources, Conservation and Recycling* 52, 747-763.

Kumar, V. (2009). "Pyrolysis and gasification of lignin and effect of alkali addition," Georgia Institute of Technology.

Li, J. (1989). "Rate process during gasification and reduction of black liquor char," Doctoral Dissertation, McGill Univ.

Lv, D. Z., Xu, M. H., Liu, X. W., Zhan, Z. H., Li, Z. Y., and Yao, H. (2010). "Effect of cellulose, lignin, alkali and alkaline earth metallic species on biomass pyrolysis and gasification," *Fuel Processing Technology* 91(8), 903-909.

Liu, Q., Wang, S., Zheng, Y., Luo, Z. Y., and Cen, K. F. (2008). "Mechanism study of wood lignin pyrolysis by using TG-FTIR analysis," *Journal of Analytical and Applied Pyrolysis* 82(1), 170-177.

Lv, G. J., Wu, S. B., Lou, R., and Yang, Q. (2010). "Analytical pyrolysis characteristics of enzymatic/mild acidolysis lignin from sugarcane bagasse," *Cellulose Chemistry and Technology* 44 (9), 335-342.

Naqvi, M., Yan, J., and Fröling, M. (2010). "Bio-refinery system of DME or CH_4 production from black liquor gasification in pulp mills." *Bioresource Technology* 101(3), 937-944.

Quyn, D. M., Wu, H. W., Bhattacharya, S. P., and Li, C. Z. (2002). "Volatilisation and catalytic effects of alkali and alkaline earth metallic species during the pyrolysis and gasification of Victorian brown coal. Part II. Effects of chemical form and valence," *Fuel* 81(2), 151-158.

Sams, D. A., and Shadman, F. (1986). "Mechanism of potassium-catalyzed carbon/CO_2 reaction," *Aiche Journal* 32, 1132-1137.

Sricharoenchaikul, V., Frederick, W. J., and Agrawal, P. (2003). "Carbon distribution in char residue from gasification of kraft black liquor," *Biomass and Bioenergy* 25(2), 209-220.

Sun, R., and Tomkinson, J. (2001). "Fractional separation and physico-chemical analysis of lignins from the black liquor of oil palm trunk fibre pulping," *Separation and Purification Technology* 24(3), 529-539.

Sharma, R. K., Wooten, J. B., Baliga, V. L., Lin, X. H., Chan, W. G., and Hajaligol, M. R. (2004). "Characterization of chars from pyrolysis of lignin," *Fuel* 83(11-12), 1469-1482.

Shi, S. L., and He, F. W., 2003. *Analysis of Pulp and Paper Making*, China Light Industry Press, Beijing.

Su, S., Li, W., Bai, Z. Q., Xiang, H. W., and Bai, J. (2010). "Production of hydrogen by steam gasification from lignin with Al_2O_3-Na_2O-H_2O/NaOH/Al(OH)$_3$ catalyst," *Journal of Fuel Chemistry and Technology* 38(3), 270-274.

Whitty, K., Backman, R., and Hupa, M. (1998). "Influence of char formation conditions on pressurized black liquor gasification rates," *Carbon* 36(11), 1683-1692.

Yang, H. P., Yan, R., and Chen, H. P. (2007). "Characteristics of hemicellulose, cellulose and lignin pyrolysis," *Fuel* 86(12-13), 1781-1788.

Yuan, T. Q., He, J., Xu, F., and Sun, R. C. (2009). "Fractionation and physico-chemical analysis of degraded lignins from the black liquor of Eucalyptus pellita KP-AQ pulping," *Polymer Degradation and Stability* 94(7), 1142-1150.

Zhu, H. M., Yan, J. H., Jiang, X. G., Lai, W. E., and Cen, K. F. (2008). "Study on pyrolysis of typical medical waste materials by using TG-FTIR analysis," *Journal of Hazardous Materials* 153(1-2), 670-676.